International Journal of Bifurcation and Chaos, Vol. 25, No. 11 (2015) 1550156 (15 pages)

DOI: 10.1142/S0218127415501564

Hopf Bifurcation Analysis of Distributed Delay Equations with Applications to Neural Networks

Franco S. Gentile*,† and Jorge L. Moiola†,‡
*Departamento de Matemática, Universidad Nacional del Sur,
B8000CPB Bahía Blanca, Argentina
†Instituto de Investigaciones en Ingeniería
Eléctrica — IIIE (UNS-CONICET),
B8000CPB Bahía Blanca, Argentina
‡Departamento de Ingeniería Eléctrica y de Computadoras,
Universidad Nacional del Sur,
B8000CPB Bahía Blanca, Argentina
*fsgentile@gmail.com
‡jmoiola@criba.edu.ar

Received April 27, 2015

In this paper, we study how to capture smooth oscillations arising from delay-differential equations with distributed delays. For this purpose, we introduce a modified version of the frequency-domain method based on the Graphical Hopf Bifurcation Theorem. Our approach takes advantage of a simple interpretation of the distributed delay effect by means of some Laplace-transformed properties. Our theoretical results are illustrated through an example of two coupled neurons with distributed delay in their communication channel. For this system, we compute several bifurcation diagrams and approximations of the amplitudes of periodic solutions. In addition, we establish analytical conditions for the appearance of a double zero bifurcation and investigate the unfolding by the proposed methodology.

Keywords: Delay-differential equation; distributed delay; Hopf bifurcation; frequency-domain method.

1. Introduction

Delay-differential equations (DDEs) often arise when modeling systems in biology, control, physics, and other research areas. Generally, in such models the delay value is assumed to be fixed, so the evolution of the state variables at time t depends on the states at moment $t - \tau$, where $\tau > 0$ is constant. However, more sophisticated models have been developed, in which all the past history of the system governs its present evolution. This dependance on a continuum of previous values of the state variables is known as distributed delay. This viewpoint allows to describe effects like uncertainties in the delay value, modification of the time lag due to unmodeled factors, probabilistic distribution of delay, etc. Consequently, in some cases the distributed delay formulation leads to more accurate models than discrete (constant) delays, generally in biological issues, as in the cellular spread of virus [Culshaw *et al.*, 2003], prey–predator systems [Ruan, 2006], epidemic models [Arino & van der Driessche, 2006], etc.

In the particular context of neural networks, the models considering distributed delays take into account the multiple connections between neurons, each with a different transmission velocity. In

addition, the utilization of distributed delays in artificial neural networks have led to very interesting applications. For example, Tank and Hopfield [1987] proposed a neural network with distributed delays for pattern recognition in time-dependent signal. Following these ideas, Unnikrishnan *et al.* [1991] used a more complex network for speech recognition. Since then, several authors focused on theoretical results about stability of neural networks with both discrete and distributed delays. Some contributions concern the global stability of an equilibrium point, generally studied by means of a Lyapunov functional, and they are applicable to huge networks (see, for example, [Gopalsamy & He, 1994; Zhang & Jin, 2000; Liu *et al.*, 2006]). However, from the point of view of bifurcations, large networks lead to untractable problems and most of the contributions in this field deal with systems consisting of a few neurons, specially when distributed delays are considered [Liao *et al.*, 2001, 2004; Ruan & Filfil, 2004; Xiao *et al.*, 2013]. Only very few authors considered relatively huge networks with multiple delays, performing bifurcation analysis using the normal form theory [Cao & Xiao, 2007] or frequency domain techniques [Yu *et al.*, 2008], although these results deal with concentrated delays.

DDEs with distributed delays are formulated as integro-differential equations, in which the influence of the past history is determined by a function called kernel or distribution. Frequently, to obtain a more tractable problem, a set of equations equivalent to the original model is attained, through defining additional variables and performing algebraic manipulations (see, for example, [Rasmussen *et al.*, 2003; Liao *et al.*, 2004; Ruan, 2006; Xiao *et al.*, 2013]). That set may involve ordinary differential equations (ODEs) as well as DDEs with discrete delays. Unfortunately, this alternative depends strongly on the characteristics of the delay distribution and sometimes it is impossible to achieve an equivalent model. If such an equivalent model is successfully attained, the analytical and numerical tools for ODEs and DDEs with constant delays are available. But, if one has to work directly with the distributed delay model, the lack of tools becomes evident.

At the best of our knowledge, the most sophisticated theoretical results on stability of DDEs with distributed delays are given in [Bernard *et al.*, 2001; Crauste, 2010; Yuan & Bélair, 2011]. Although those only refer to scalar equations, they provide the very key ideas to understand the effects of the delay distribution over stability. For nonscalar equations, the numerical results in [Atay, 2003] give important insights about the effect of the spread of the delay distribution on the dynamics of coupled oscillators.

In this article, we propose a modified version of the method based on the Graphical Hopf Bifurcation Theorem (GHBT for short) [Mees & Chua, 1979; Moiola & Chen, 1996] for analyzing bifurcations in DDEs with distributed delays. This approach is a generalization of the one presented in [Gentile *et al.*, 2012] for systems with discrete delays. The development of this technique does not depend on the particular shape of the distribution function, and we only require less restrictive conditions from it. Our setting shows that the effect of the delay distribution can be described simply by using properties of the Laplace transform. Moreover, the methodology can be applied to systems with any number of state variables, not only to scalar equations.

There are several contributions concerning the bifurcation analysis of neural networks with distributed delays using the GHBT. Liao *et al.* [2003] studied a two-neuron system with a weak gamma kernel. Later, Liao *et al.* [2004] analyzed a similar network but considering a strong gamma kernel. Hajihosseini *et al.* [2010] considered a three-neuron network with a strong gamma kernel too. More recently, Xiao *et al.* [2013] carried out a bifurcation analysis of a two-neuron system with a weak kernel, but they considered not only delayed connections between the different neurons but also self-connections in each neuron. In these articles, the authors used the chain trick to derive equivalent models expressed as ODEs. For example, in [Liao *et al.*, 2004] the two-neuron model with a strong gamma kernel is rewritten as a system of six ODEs before applying the GHBT. In [Hajihosseini *et al.*, 2010] the three-neuron network with a weak kernel is also transformed into a system of six ODEs. But, for instance, if a uniform distribution is used in those examples, the equivalent models are no longer given by systems of ODEs but by systems of DDEs, and the bifurcation analysis changes drastically. As will be shown in the following sections, our proposal is distinguished from the previous works by the fact that we will not need to transform the original system into an equivalent one. That is to say, our goal is to establish a procedure which could be carried out

independently from the kernel used in the model. Although the base of the method proposed here is the same as that in the mentioned works, a subtle difference in the representation of the distributed delay makes the calculation procedure noticeably different from the previous results.

The paper is organized as follows. In Sec. 2, we propose a modified version of the technique based on the GHBT to study distributed delay equations. In Sec. 3, we illustrate our results with an example of coupled neurons, for which several bifurcation diagrams are found. In addition, for this example we obtain approximations of the amplitude of the periodic solutions emerging from Hopf bifurcations. Analytical conditions for the appearance of a double zero bifurcation are also found. The dynamics generated by the double zero are studied in some detail for a particular choice of the activation function of the neurons. Finally, the conclusions of the paper are given in Sec. 4.

2. Alternative Formulation for DDEs with Distributed Delays

The general form of a DDE with distributed delay can be stated as follows

$$\dot{\mathbf{x}}(t) = \mathbf{f}\left[\mathbf{x}(t), \int_{-\infty}^{t} \mathbf{x}(u)k(t-u)du; \mu\right], \quad (1)$$

where $\mathbf{x} \in \mathbb{R}^n$, $\mu \in \mathbb{R}$ is the bifurcation parameter, $\mathbf{f} : \mathbb{R}^n \times \mathbb{R}^n \times \mathbb{R} \to \mathbb{R}^n$ is a smooth nonlinear functional and $k(\cdot)$ is the (scalar) distribution function, which weighs the past values of $\mathbf{x}$ and verifies

$$k(u) \geq 0, \quad \forall\, u \in [0, \infty); \quad \int_0^\infty k(u)du = 1. \quad (2)$$

Also, the *mean delay* τ_m is defined as

$$\tau_m \triangleq \int_0^\infty uk(u)du. \quad (3)$$

Notice that the integral in (1) is not necessarily improper, because $k(\cdot)$ may have finite support. Equation (1) has been studied by many authors, mostly in biological applications (see, for example, [Culshaw *et al.*, 2003; Ruan & Filfil, 2004; Arino & van der Driessche, 2006]). In order to deal with integro-differential equations like (1), the most common approach is to find an equivalent system, formulated as a set of ODEs and/or DDEs (generally using the chain trick and avoiding the explicitness of integral terms; see, for example, [Culshaw *et al.*, 2003; Rasmussen *et al.*, 2003; Liao *et al.*, 2004; Xiao *et al.*, 2013]). But this trick has an important disadvantage: the number of additional equations that must be introduced and their kind (ODEs or DDEs) depend strongly on the particular shape of the kernel. Moreover, that trick can be applied only for particular cases of the distribution function, for example, the gamma and uniform waveforms, but not for general distributions.

In this work, we propose a modified version of the method based on the GHBT developed in [Mees & Chua, 1979; Moiola & Chen, 1996] for studying Hopf bifurcations in equations like (1). The most important advantage of our approach is that the effect of the distributed delay is represented easily through properties of the Laplace transform, which is the mathematical framework in which the GHBT was developed. Then, the goal is to study not only models which can be reduced to an equivalent set of ODEs or DDEs, but also every model in which the kernel function has a Laplace transform. Let us choose adequate matrices $A \in \mathbb{R}^{n\times n}$, $B \in \mathbb{R}^{n\times p}$ and $C \in \mathbb{R}^{m\times n}$, then Eq. (1) can be recast in the feedback form

$$\begin{cases} \dot{\mathbf{x}}(t) = A\mathbf{x}(t) + B\mathbf{g}[\mathbf{y}(t), \mathbf{y}_k(t); \mu], \\ \mathbf{y}(t) = -C\mathbf{x}(t), \end{cases} \quad (4)$$

where

$$\mathbf{y}_k(t) \triangleq \int_{-\infty}^{t} \mathbf{y}(u)k(t-u)du. \quad (5)$$

By applying the Laplace transform to (4) (with zero initial conditions), we have

$$\begin{aligned} \mathcal{L}\{\mathbf{x}(t)\} &= (sI_n - A)^{-1}B\mathcal{L}\{\mathbf{g}[\mathbf{y}(t), \mathbf{y}_k(t); \mu]\}, \\ \mathcal{L}\{\mathbf{y}(t)\} &= -C\mathcal{L}\{\mathbf{x}(t)\} \\ &= -G(s;\mu)\mathcal{L}\{\mathbf{g}[\mathbf{y}(t), \mathbf{y}_k(t); \mu]\}, \end{aligned} \quad (6)$$

where $s \in \mathbb{C}$, I_n denotes the $n \times n$ identity matrix[1] and

$$G(s;\mu) \triangleq C(sI_n - A)^{-1}B \quad (7)$$

is a transfer function representing a linear subsystem of (4),[2] as can be seen in Fig. 1(a). From the

[1]A similar notation for other identity matrices will be used hereinafter.

[2]By using the notation $G(s;\mu)$ we emphasize the usual dependence of matrices A, B and C on the parameter μ.

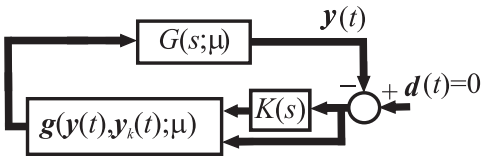

(a)

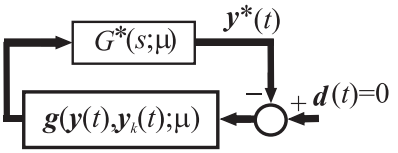

(b)

Fig. 1. (a) Block representation of system (4) and (b) equivalent system with the extended matrix $G^*(s;\mu)$.

convolution property, for the "retarded" quantities, we have

$$\begin{aligned}\mathcal{L}\{\mathbf{x}_k(t)\} &= \mathcal{L}\{\mathbf{x}(t)\}K(s),\\ \mathcal{L}\{\mathbf{y}_k(t)\} &= -C\mathcal{L}\{\mathbf{x}_k(t)\} = -C\mathcal{L}\{\mathbf{x}(t)\}K(s),\end{aligned} \tag{8}$$

where $K(s) \triangleq \mathcal{L}\{k(t)\}$. Notice that conditions (2) imply that the Laplace transform $K(s)$ exists at least for $\Re\{s\} > 0$. System (4) is represented in Fig. 1(a). Notice that both $\mathbf{y}(t)$ and $\mathbf{y}_k(t)$ act as inputs of the nonlinear block $\mathbf{g}[\cdot]$. In order to apply the GHBT method described in [Mees & Chua, 1979; Moiola & Chen, 1996], we would like to find an equivalent block representation consisting of a single linear system with a nonlinear feedback function. This goal can be achieved by defining an extended matrix

$$G^*(s;\mu) \triangleq \begin{pmatrix} G(s;\mu) \\ G(s;\mu)K(s) \end{pmatrix} \in \mathbb{R}^{2m\times p}, \tag{9}$$

thus absorbing the delay block into the forward path as shown in Fig. 1(b), where $\mathbf{y}^*(t)$ denotes the "extended" output

$$\mathbf{y}^*(t) \triangleq \begin{pmatrix} \mathbf{y}(t) \\ \mathbf{y}_k(t) \end{pmatrix} \in \mathbb{R}^{2m}. \tag{10}$$

Moreover, the methodology described in [Mees & Chua, 1979; Moiola & Chen, 1996] can be applied without further modifications. In order to detect bifurcations, the nonlinear feedback block is linearized by computing the Jacobian matrix

$$J^*(\mu) = \left(\frac{\partial \mathbf{g}(\mathbf{y},\mathbf{y}_k;\mu)}{\partial \mathbf{y}} \,\middle|\, \frac{\partial \mathbf{g}(\mathbf{y},\mathbf{y}_k;\mu)}{\partial \mathbf{y}_k} \right)\Bigg|_{\mathbf{y}^*=\hat{\mathbf{y}}^*}. \tag{11}$$

Notice that both derivatives above are themselves Jacobian matrices with respect to $\mathbf{y}$ and $\mathbf{y}_k$ and $J^*(\mu) \in \mathbb{R}^{p\times 2m}$. All the formulae of the classic GHBT method remain valid, with the obvious dimensional augmentation of matrices and vectors. In order to provide a more rigorous justification for this assertion, let us consider the Fourier representation of the output proposed by Mees and Chua [1979]

$$\mathbf{y}_k(t) \sim \hat{\mathbf{y}} + \Re\left\{\sum_{r=0}^{2} \mathcal{Y}^r e^{ir\omega t}\right\},$$

then for the delayed output $\mathbf{y}_k(t)$ we have

$$\begin{aligned}\mathbf{y}_k(t) &\sim \int_{-\infty}^{t} \left[\hat{\mathbf{y}} + \Re\left\{\sum_{r=0}^{2} \mathcal{Y}^r e^{ir\omega u}\right\}\right] k(t-u)du\\ &= \hat{\mathbf{y}} + \Re\left\{\sum_{r=0}^{2} \mathcal{Y}^r \int_{-\infty}^{t} e^{ir\omega u}k(t-u)du\right\}\\ &= \hat{\mathbf{y}} + \Re\left\{\sum_{r=0}^{2} \mathcal{Y}^r e^{ir\omega t}\int_{0}^{\infty} e^{-ir\omega u}k(u)du\right\}\\ &= \hat{\mathbf{y}} + \Re\left\{\sum_{r=0}^{2} \mathcal{Y}^r K(i\omega r)e^{ir\omega t}\right\}.\end{aligned}$$

Thus, the rth Fourier coefficient of $\mathbf{y}_k(t)$ is given by the rth Fourier coefficient of $\mathbf{y}_k(t)$ times $K(i\omega r)$. By defining $\mathbf{e}(t) \triangleq \mathbf{y}(t) - \hat{\mathbf{y}}$ and $\mathbf{e}_k(t) \triangleq \mathbf{y}_k(t) - \hat{\mathbf{y}}$, we can compute the Taylor series of the nonlinear function $\mathbf{g}[\cdot]$ as

$$\begin{aligned}\mathbf{g}[\cdot] \simeq\ & \mathbf{g}[\hat{\mathbf{y}},\hat{\mathbf{y}};\mu] + (D_1^1\mathbf{g})\mathbf{e} + (D_2^1\mathbf{g})\mathbf{e}_k\\ &+ \frac{1}{2}(D_{11}^2\mathbf{g})\mathbf{e}\otimes\mathbf{e} + (D_{12}^2\mathbf{g})\mathbf{e}\otimes\mathbf{e}_k\\ &+ \frac{1}{2}(D_{22}^2\mathbf{g})\mathbf{e}_k\otimes\mathbf{e}_k + \frac{1}{3!}(D_{111}^3\mathbf{g})\mathbf{e}\otimes\mathbf{e}\otimes\mathbf{e}\\ &+ (D_{112}^3\mathbf{g})\mathbf{e}\otimes\mathbf{e}\otimes\mathbf{e}_k + (D_{122}^3\mathbf{g})\mathbf{e}\otimes\mathbf{e}_k\otimes\mathbf{e}_k\\ &+ \frac{1}{3!}(D_{222}^3\mathbf{g})\mathbf{e}_k\otimes\mathbf{e}_k\otimes\mathbf{e}_k + \mathcal{O}(|\mathbf{e}|^4),\end{aligned} \tag{12}$$

where we have suppressed the argument t for short and the derivatives are defined as

$$(\mathbf{D}^2_{ij}\mathbf{g}) \triangleq \left.\frac{\partial \mathbf{g}^2(\mathbf{y}_1,\mathbf{y}_2;\mu)}{\partial \mathbf{y}_i \partial \mathbf{y}_j}\right|_{(\mathbf{y}_1,\mathbf{y}_2)=(\hat{\mathbf{y}},\hat{\mathbf{y}})} \in \mathbb{R}^{p\times(2m)^2},$$

$$(\mathbf{D}^3_{ijk}\mathbf{g}) \triangleq \left.\frac{\partial \mathbf{g}^3(\mathbf{y}_1,\mathbf{y}_2;\mu)}{\partial \mathbf{y}_i \partial \mathbf{y}_j \partial \mathbf{y}_k}\right|_{(\mathbf{y}_1,\mathbf{y}_2)=(\hat{\mathbf{y}},\hat{\mathbf{y}})} \in \mathbb{R}^{p\times(2m)^3}, \tag{13}$$

where $i,j,k = 1$ or 2. Let us introduce the compact notation $K_n \triangleq K(in\omega)$. Thus, for example, the term $\mathbf{e}\otimes\mathbf{e}_k$ in (12) is given by

$$\begin{aligned}\mathbf{e}\otimes\mathbf{e}_k = {}& \frac{1}{4}\mathcal{Y}^1\otimes\overline{\mathcal{Y}}^1 K_1 + \frac{1}{4}\overline{\mathcal{Y}}^1\otimes\mathcal{Y}^1\overline{K}_1\\ &+\frac{1}{2}\mathcal{Y}^0\otimes\mathcal{Y}^1 e^{i\omega t}+\frac{1}{2}\mathcal{Y}^0\otimes\overline{\mathcal{Y}}^1 e^{-i\omega t}\\ &+\frac{1}{2}\mathcal{Y}^0\otimes\mathcal{Y}^1 K_1 e^{i\omega t}+\frac{1}{2}\mathcal{Y}^0\otimes\overline{\mathcal{Y}}^1\overline{K}_1 e^{-i\omega t}\\ &+\frac{1}{4}\overline{\mathcal{Y}}^1\otimes\mathcal{Y}^2\overline{K}_1 e^{i\omega t}+\frac{1}{4}\mathcal{Y}^1\otimes\overline{\mathcal{Y}}^2 K_1 e^{-i\omega t}\\ &+\frac{1}{4}\overline{\mathcal{Y}}^1\otimes\mathcal{Y}^2 K_2 e^{i\omega t}+\frac{1}{4}\mathcal{Y}^1\otimes\overline{\mathcal{Y}}^2\overline{K}_2 e^{-i\omega t}\\ &+\frac{1}{4}\mathcal{Y}^1\otimes\mathcal{Y}^1 K_1 e^{i2\omega t}+\frac{1}{4}\overline{\mathcal{Y}}^1\otimes\overline{\mathcal{Y}}^1\overline{K}_1 e^{-i2\omega t}\\ &+\frac{1}{4}\mathcal{Y}^1\otimes\mathcal{Y}^2 K_1 e^{i3\omega t}+\frac{1}{4}\overline{\mathcal{Y}}^1\otimes\overline{\mathcal{Y}}^2\overline{K}_1 e^{-i3\omega t}\\ &+\frac{1}{4}\mathcal{Y}^1\otimes\mathcal{Y}^2 K_2 e^{i3\omega t}+\frac{1}{4}\overline{\mathcal{Y}}^1\otimes\overline{\mathcal{Y}}^2\overline{K}_2 e^{-i3\omega t}\\ &+\mathcal{O}(|\mathbf{e}|^4).\end{aligned} \tag{14}$$

Replacing all terms like (14) into (12), we obtain the expansion of $\mathbf{g}[\cdot]$ in powers of the Fourier coefficients $\mathcal{Y}^r$. As the fundamental frequency of $\mathbf{y}(t)$ is ω, then the fundamental frequency of $\mathbf{g}[\mathbf{y}(t), \mathbf{y}_k(t);\mu]$ is also ω. Then, for this nonlinear function we have

$$\mathbf{g}[\mathbf{y}(t),\mathbf{y}_k(t);\mu] \simeq \mathbf{g}[\hat{\mathbf{y}},\hat{\mathbf{y}};\mu] + \Re\left\{\sum_{r=0}^{2}\mathcal{G}^r e^{i\omega r t}\right\}.$$

Grouping together terms of the same frequency in (12), after some calculations we find

$$\begin{aligned}\mathcal{G}^0 = {}& (D^1_1\mathbf{g})\mathcal{Y}^0 + (D^1_2\mathbf{g})\mathcal{Y}^0 + \frac{1}{4}(D^2_{11}\mathbf{g})\mathcal{Y}^1\otimes\overline{\mathcal{Y}}^1\\ &+\frac{1}{4}(D^2_{22}\mathbf{g})\mathcal{Y}^1\otimes\overline{\mathcal{Y}}^1 K_1\overline{K}_1 + \frac{1}{4}(D^2_{12}\mathbf{g})\\ &\times[\mathcal{Y}^1\otimes\overline{\mathcal{Y}}^1 K_1 + \overline{\mathcal{Y}}^1\otimes\mathcal{Y}^1\overline{K}_1] + O(|\mathcal{Y}^1|^4),\end{aligned} \tag{15}$$

$$\begin{aligned}\mathcal{G}^1 = {}& (D^1_1\mathbf{g})\mathcal{Y}^1 + (D^1_2\mathbf{g})\mathcal{Y}^1 K_1\\ &+(D^2_{11}\mathbf{g})\left[\mathcal{Y}^0\otimes\mathcal{Y}^1+\frac{1}{2}\overline{\mathcal{Y}}^1\otimes\mathcal{Y}^2\right]\\ &+(D^2_{12}\mathbf{g})\left[\mathcal{Y}^0\otimes\mathcal{Y}^1+\mathcal{Y}^0\otimes\mathcal{Y}^1 K_1\right.\\ &\left.+\frac{1}{2}\overline{\mathcal{Y}}^1\otimes\mathcal{Y}^2\overline{K_1}+\frac{1}{2}\overline{\mathcal{Y}}^1\otimes\mathcal{Y}^2 K_2\right]\\ &+(D^2_{22}\mathbf{g})\left[\mathcal{Y}^0\otimes\mathcal{Y}^1 K_1+\frac{1}{2}\overline{\mathcal{Y}}^1\otimes\mathcal{Y}^2\overline{K}_1 K_2\right]\\ &+\frac{1}{8}(D^3_{111}\mathbf{g})\mathcal{Y}^1\otimes\mathcal{Y}^1\otimes\overline{\mathcal{Y}}^1\\ &+\frac{1}{2}(D^3_{112}\mathbf{g})\left[\mathcal{Y}^1\otimes\mathcal{Y}^1\otimes\overline{\mathcal{Y}}^1 K_1\right.\\ &\left.+\frac{1}{2}\mathcal{Y}^1\otimes\overline{\mathcal{Y}}^1\otimes\mathcal{Y}^1\overline{K}_1\right]\\ &+\frac{1}{2}(D^3_{122}\mathbf{g})\left[\mathcal{Y}^1\otimes\mathcal{Y}^1\otimes\overline{\mathcal{Y}}^1|K_1|^2\right.\\ &\left.+\frac{1}{2}\mathcal{Y}^1\otimes\mathcal{Y}^1\otimes\overline{\mathcal{Y}}^1 K_1^2\right]+\frac{1}{8}(D^3_{222}\mathbf{g})\mathcal{Y}^1\\ &\otimes\mathcal{Y}^1\otimes\overline{\mathcal{Y}}^1 K_1^2\overline{K}_1 + O(|\mathcal{Y}^1|^4),\end{aligned} \tag{16}$$

$$\begin{aligned}\mathcal{G}^2 = {}& (D^1_1\mathbf{g})\mathcal{Y}^2 + (D^1_2\mathbf{g})\mathcal{Y}^2 K_2\\ &+\frac{1}{4}(D^2_{11}\mathbf{g})\mathcal{Y}^1\otimes\mathcal{Y}^1+\frac{1}{2}(D^2_{12}\mathbf{g})\mathcal{Y}^1\otimes\mathcal{Y}^1 K_1\\ &+\frac{1}{4}(D^2_{22}\mathbf{g})\mathcal{Y}^1\otimes\mathcal{Y}^1 K_1^2 + O(|\mathcal{Y}^1|^4).\end{aligned} \tag{17}$$

Then, if we define the "augmented" Fourier coefficients

$$\mathcal{Y}^{n*} \triangleq \begin{pmatrix}\mathcal{Y}^n\\ \mathcal{Y}^n K_n\end{pmatrix}, \quad n=0,1,2,$$

for example, Eq. (15) can be expressed as

$$\mathcal{G}^0 = J^*(\mu)\mathcal{Y}^{0*} + \frac{1}{4}(\mathfrak{D}^2\mathbf{g})\mathcal{Y}^{1*}\otimes\overline{\mathcal{Y}}^{1*}, \tag{18}$$

where $J^*(\mu)$ was defined in (11),

$$(\mathfrak{D}^2\mathbf{g}) \triangleq (D^2_{11}\mathbf{g}\,|\,D^2_{12}\mathbf{g}\,|\,D^2_{21}\mathbf{g}\,|\,D^2_{22}\mathbf{g}) \in \mathbb{R}^{p\times(2m)^2} \tag{19}$$

and

$$\mathcal{Y}^{1*} \otimes \overline{\mathcal{Y}}^{1*} = \begin{pmatrix} \mathcal{Y}^1 \otimes \overline{\mathcal{Y}}^1 \\ \mathcal{Y}^1 \otimes \overline{\mathcal{Y}}^1 \overline{K}_1 \\ \mathcal{Y}^1 \otimes \overline{\mathcal{Y}}^1 K_1 \\ \mathcal{Y}^1 \otimes \overline{\mathcal{Y}}^1 |K_1|^2 \end{pmatrix} \in \mathbb{R}^{(2m)^2 \times 1}.$$

Similarly, $\mathcal{G}^2$ in (17) becomes

$$\mathcal{G}^2 = J^*(\mu)\mathcal{Y}^{2*} + \frac{1}{4}(\mathfrak{D}^2\mathbf{g})\mathcal{Y}^{1*} \otimes \mathcal{Y}^{1*}, \tag{20}$$

and finally, $\mathcal{G}^1$ in (16) can be expressed compactly as

$$\mathcal{G}^1 = J^*(\mu)\mathcal{Y}^{1*} + (\mathfrak{D}^2\mathbf{g})[\mathcal{Y}^{0*} \otimes \mathcal{Y}^{1*} + \overline{\mathcal{Y}}^{1*} \otimes \mathcal{Y}^{2*}] + \frac{1}{8}(\mathfrak{D}^3\mathbf{g})\mathcal{Y}^{1*} \otimes \mathcal{Y}^{1*} \otimes \overline{\mathcal{Y}}^{1*}, \tag{21}$$

where

$$(\mathfrak{D}^3\mathbf{g}) \triangleq (D^3_{111}\mathbf{g} \,|\, D^3_{112}\mathbf{g} \,|\, \cdots \,|\, D^3_{222}\mathbf{g}) \in \mathbb{R}^{p \times 8m^3}.$$

Moreover, the input and the output of the linear block in Fig. 1(b) verify the following second-order harmonic balance equation

$$\mathcal{Y}^{r*} = -G^*(ir\omega;\mu)\mathcal{G}^r \quad r = 0, 1, 2. \tag{22}$$

Thus, by using the equation above in (18) and (20), we obtain

$$\begin{aligned} \mathcal{Y}^{0*} &= -\frac{1}{4}H(0;\mu)(\mathfrak{D}^2\mathbf{g})\mathcal{Y}^{1*} \otimes \overline{\mathcal{Y}}^{1*}, \\ \mathcal{Y}^{2*} &= -\frac{1}{4}H(i2\omega;\mu)(\mathfrak{D}^2\mathbf{g})\mathcal{Y}^{1*} \otimes \mathcal{Y}^{1*}, \end{aligned} \tag{23}$$

where

$$H^*(s;\mu) \triangleq [G^*(s;\mu)J^*(\mu) + I_{2m}]^{-1}G^*(s;\mu). \tag{24}$$

From (21) and using (22) again, the equation for $\mathcal{Y}^{1*}$ becomes

$$[I_{2m} + G^*(i\omega;\mu)J^*(\mu)]\mathcal{Y}^{1*} = -G^*(i\omega;\mu)\mathbf{p}(\omega;\mathcal{Y}^{1*}), \tag{25}$$

where

$$\mathbf{p}(\omega;\mathcal{Y}^{1*}) \triangleq (\mathfrak{D}^2\mathbf{g})[\mathcal{Y}^{0*} \otimes \mathcal{Y}^{1*} + \overline{\mathcal{Y}}^{1*} \otimes \mathcal{Y}^{2*}] + \frac{1}{8}(\mathfrak{D}^3\mathbf{g})\mathcal{Y}^{1*} \otimes \mathcal{Y}^{1*} \otimes \overline{\mathcal{Y}}^{1*}. \tag{26}$$

Following the same procedure as by Mees and Chua [1979], it is found that the existence of a periodic solution in system (4) is subject to the existence of a solution (ω, θ) of the equation

$$\hat{\lambda}(i\omega;\mu) + 1 = \theta^2\xi(\omega;\mu) + \mathcal{O}(\theta^3), \tag{27}$$

where $\theta \geq 0$ is a measure of the amplitude of the oscillation,

$$\xi(\omega;\mu) \triangleq -\frac{\mathbf{u}^T G^*(i\omega;\mu)\mathbf{p}(\omega,\mathbf{v})}{\mathbf{u}^T\mathbf{v}}, \tag{28}$$

$\mathbf{u}$, $\mathbf{v}$ are the left and right eigenvectors of $G^*(i\omega;\mu)J^*(\mu)$ and $\mathbf{p}(\omega,\mathbf{v}) = \mathbf{p}(\omega;\mathcal{Y}^{1*})/\theta^2$ (see [Mees & Chua, 1979; Moiola & Chen, 1996]). In conclusion, we arrived at the formulae analogous to that presented in [Mees & Chua, 1979; Moiola & Chen, 1996], with the obvious augmentation in the dimension of matrices and vectors. The effect of the delay distribution is taken into account into the linear part by considering the extended transfer function $G^*(s;\mu)$.

Remark. Notice that a constant (concentrated) delay of τ units of time can be easily obtained by taking $k(u) = \delta(u - \tau)$ in (1), where $\delta(\cdot)$ is the Dirac delta distribution. This particular case was studied in [Gentile *et al.*, 2012].

3. Example: Two Neurons with Delayed Coupling

In this section, we will study an example presented in [Liao *et al.*, 2001], consisting of two coupled neurons in which the connections between them are affected by distributed delays. Even though models based on distributed delays are thought for large scale networks, it is important to understand first the effect of the spread of delays in a relatively simple system. Let us consider the following model

$$\begin{aligned} &\begin{cases} \dot{x}_1(t) = -x_1(t) + a_1 f[x_2(t) - b_2 x_{2k}(t)], \\ \dot{x}_2(t) = -x_2(t) + a_2 f[x_1(t) - b_1 x_{1k}(t)], \end{cases} \\ &x_{ik}(t) \triangleq \int_{-\infty}^{t} k(t-u)x_i(u)du, \quad i = 1, 2, \end{aligned} \tag{29}$$

where $a_i, b_i \geq 0$. Here, $x_i(t)$ represents the mean sum potential of the neuron, a_i denotes the range of the variables x_i, and b_i are measures of the inhibitory influence of the past history. We assume that the nonlinear activation function $f(\cdot)$ is smooth and verifies $f(0) = 0$, $f' \triangleq f'(0) > 0$. We also assume that the kernel function satisfies conditions (2).

In order to apply the formulation given in Sec. 2, for the feedback system representation we choose

$$A = -I_2, \quad B = C = I_2,$$
$$\mathbf{g}[\mathbf{y}^*(t);\mu] = \begin{pmatrix} a_1 f(b_2 y_{2k} - y_2) \\ a_2 f(b_1 y_{1k} - y_1) \end{pmatrix}, \tag{30}$$

where $y_{ik}(t) := -x_{ik}(t)$ and $\mu \triangleq (a_1, a_2, b_1, b_2)$ is a vector of parameters. From (7) and (9), the linear part of the feedback system [see Fig. 1(a)] is represented by the transfer matrix

$$G^*(s) = \begin{pmatrix} G(s) \\ G(s)K(s) \end{pmatrix}, \quad G(s) = \frac{1}{s+1} I_2. \tag{31}$$

The equilibrium points of (29) are defined implicitly by the equations

$$\begin{cases} \hat{x}_1 = a_1 f[(1-b_2)\hat{x}_2], \\ \hat{x}_2 = a_2 f[(1-b_1)\hat{x}_1]. \end{cases} \tag{32}$$

As $f(0) = 0$, it follows that $(\hat{x}_1, \hat{x}_2) = (0, 0)$ is a trivial equilibrium point of (29). However, depending on the particular shape of function $f(\cdot)$ and the values of parameters a_1, a_2, b_1 and b_2, other nontrivial equilibrium points may also exist if $b_1 \neq 1$ and $b_2 \neq 1$. We will deal mainly with the bifurcations exhibited by the trivial equilibrium point. However, at the end of this section we shall consider a particular function $f(\cdot)$ in (29), find other equilibria and also study their dynamics. From (11), the linearization of the nonlinear feedback function around the trivial equilibrium point $\hat{\mathbf{y}}^* = 0$ is given by

$$J^*(\mu) = f' \begin{pmatrix} 0 & -a_1 & 0 & a_1 b_2 \\ -a_2 & 0 & a_2 b_1 & 0 \end{pmatrix}. \tag{33}$$

As explained in [Mees & Chua, 1979; Moiola & Chen, 1996], the bifurcation condition can be found seeking for solutions of the following equation, which is called characteristic equation in the frequency domain

$$\begin{aligned} h(\lambda, s; \mu) &= |\lambda I_4 - G^*(s) J^*(\mu)| \\ &= \frac{\lambda^2}{(s+1)^2} \{\lambda^2 (s+1)^2 \\ &\quad - a_1 a_2 (f')^2 \eta_1(s) \eta_2(s)\} = 0, \end{aligned} \tag{34}$$

where

$$\eta_j(s) \triangleq b_j K(s) - 1, \quad j = 1, 2. \tag{35}$$

Basically, if an eigenvalue of the matrix of linearization of system (1) around an equilibrium point $\hat{\mathbf{x}}$, assumes a purely imaginary value $i\omega_0$ at a particular value $\mu = \mu_0$, then a solution $\lambda = \lambda(s;\mu)$ of (34) must assume the value $-1 + i0$ at $\mu = \mu_0$ with $s = i\omega_0$. If $\omega_0 = 0$ the bifurcation is called *static* and if $\omega_0 \neq 0$ the bifurcation is called *dynamic* or *Hopf*.

3.1. *Analysis of static bifurcations*

As mentioned above, the static bifurcations (or bifurcations of equilibria) are detected in the parameter space seeking for solutions of

$$h(-1, 0; \mu) = 0. \tag{36}$$

By considering (34) and taking into account that $K(0) = 1$ [from (2)], the equation above becomes

$$h(-1, 0; \mu) = 1 - \delta^2 (b_1 - 1)(b_2 - 1) = 0, \tag{37}$$

where $\delta \triangleq \sqrt{a_1 a_2} f'$. So, the condition for a static bifurcation can be stated as

$$\delta_{ST} = \frac{1}{\sqrt{(b_1 - 1)(b_2 - 1)}}, \quad (b_1 - 1)(b_2 - 1) \neq 1. \tag{38}$$

In addition, we can look for multiple solutions of Eq. (36) at $s = 0$. It is simple to show that

$$\begin{aligned} \frac{\partial h}{\partial s} = \frac{\lambda^2 \delta^2}{(s+1)^3} \{ & 2\eta_1(s)\eta_2(s) - (s+1)K'(s) \\ & \times [b_1 \eta_2(s) + b_2 \eta_1(s)]\}, \end{aligned}$$

where $K'(s) \triangleq dK(s)/ds$. Then, in order to have $\partial h/\partial s|_{s=0} = 0$, the following equation must be satisfied

$$b_1 b_2 [1 - K'(0)] - (b_1 + b_2) \left[1 - \frac{K'(0)}{2}\right] + 1 = 0.$$

In addition, taking into account (3), we have

$$K'(0) = -\int_0^\infty u k(u) du = -\tau_m$$

and the condition for a double root of $h(-1, s; \mu)$ at $s = 0$ can be stated in terms of the mean delay as

$$\tau_m^{(\mathrm{DZ})} = -1 + \frac{b_1 + b_2 - 2}{2b_1 b_2 - b_1 - b_2}, \tag{39}$$

where the superscript DZ denotes a double zero bifurcation. In general, if the right-hand expression in Eq. (39) is positive, the system is likely to exhibit a DZ bifurcation for an appropriate value of the mean delay. In Fig. 2, the shaded region corresponds to pairs (b_1, b_2) for which $\tau_m^{(\mathrm{DZ})}$ defined by (39) is positive. Note that the potential occurrence of a DZ

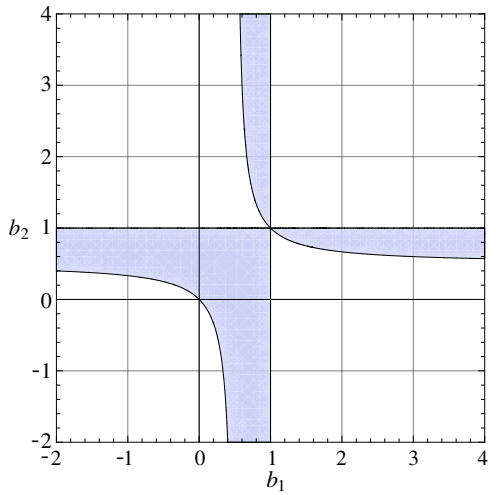

Fig. 2. The shaded area represents the feasible pairs (b_1, b_2) for which a DZ bifurcation can exist.

bifurcation depends only on the weights of the past histories and the mean delay, not on the particular shape of the distribution neither on the parameters a_1 and a_2. As can be seen in Fig. 2, the DZ bifurcation cannot exist if $b_1, b_2 < 0$ (i.e. if the past history has an excitatory effect on both neurons), but it can occur for cases in which one past history is excitatory and the other inhibitory, and for cases in which both histories have inhibitory effects.

3.2. *Analysis of Hopf bifurcation*

Equation (34) has a solution $\hat{\lambda}(s;\mu)$ given by

$$\hat{\lambda}(s;\mu) = \frac{\delta\sqrt{\eta_1(s)}\sqrt{\eta_2(s)}}{s+1}, \tag{40}$$

where $\eta_1(s)$ and $\eta_2(s)$ are defined in (35). Notice that the equation above allows studying asymmetries in the two kernels. This is important because the delays of the two communication paths between neurons may have different distributions. Taking into account Lemma 1 and (40), the Hopf bifurcation condition $\hat{\lambda}(i\omega_0;\mu_0) = -1$ can be expressed as

$$(1+i\omega_0)^2 - \delta^2\eta_1(i\omega_0)\eta_2(i\omega_0) = 0. \tag{41}$$

In order to show a concrete example, let us choose a particular kernel $k(\cdot)$. As in [Liao *et al.*, 2001], we consider a gamma distribution given by

$$k_a^p(u) = \frac{a^p u^{p-1} e^{-au}}{(p-1)!}, \quad u \geq 0. \tag{42}$$

In the cited text, the authors used the so-called *weak* kernel, obtained from (42), taking $p = 1$. They studied the Hopf bifurcations arising in system (29) through the normal form theory. In [Liao *et al.*, 2004] the authors studied system (29) by considering the *strong* gamma kernel ($p = 2$). They used the GHBT method but previously transforming model (29) into an equivalent system of six ODEs.

For the gamma kernel (42), we have

$$K_a^p(s) = \frac{a^p}{(s+a)^p} \tag{43}$$

and the Hopf bifurcation condition (41) can be expressed as

$$(1+i\omega_0)^2(a+i\omega_0)^{2p} - \delta^2[b_1 a^p - (a+i\omega_0)^p] \times [b_2 a^p - (a+i\omega_0)^p] = 0. \tag{44}$$

For example, for the *weak* kernel ($p = 1$), the equation above becomes

$$(1+i\omega_0)^2(a+i\omega_0)^2 - \delta^2[ab_1^* - i\omega_0][ab_2^* - i\omega_0] = 0,$$

where $b_1^* \triangleq b_1 - 1$ and $b_2^* \triangleq b_2 - 1$. Splitting into real and imaginary parts as before, we obtain

$$\begin{cases} (a^2-\omega_0^2)(1-\omega_0^2) - 4a\omega_0^2 - \delta^2(a^2 b_1^* b_2^* - \omega_0^2) = 0 \\ 2[a^2 - \omega_0^2 + a(1-\omega_0^2)] + a\delta^2(b_1^* + b_2^*) = 0. \end{cases} \tag{45}$$

From the second equation we can solve for the critical frequency as $\omega_0^2 = a[1 + \delta^2(b_1^* + b_2^*)/[2(a+1)]]$, and replacing into the first one, we obtain the equation representing the Hopf points in the parameter space as

$$b_m[a(b_m+1)+1]\delta^4 - (a+1)^4 - (a+1)^2 \times [ab_1^* b_2^* + (a+1)b_m - 1]\delta^2 = 0, \tag{46}$$

where $b_m \triangleq (b_1^* + b_2^*)/2$. For example, taking fixed values of b_1^* and b_2^*, we can find the Hopf curve in the (δ, a) space from (46). Figure 3 shows several bifurcation diagrams obtained with $b_2 = 1/2$ and different fixed values of b_1. The curve representing a static bifurcation is obtained from (38) and the Hopf bifurcation curve is given implicitly by (46), which can be plotted using a standard software such as Mathematica. In each Hopf curve, H indicates that the Hopf bifurcation is supercritical along it. This means that a stable limit cycle emerges when the equilibrium point at the origin switches from stable to unstable. In addition, the Hopf curve collides with the static one at the DZ point, as is very well known [Kuznetsov, 2004]. For

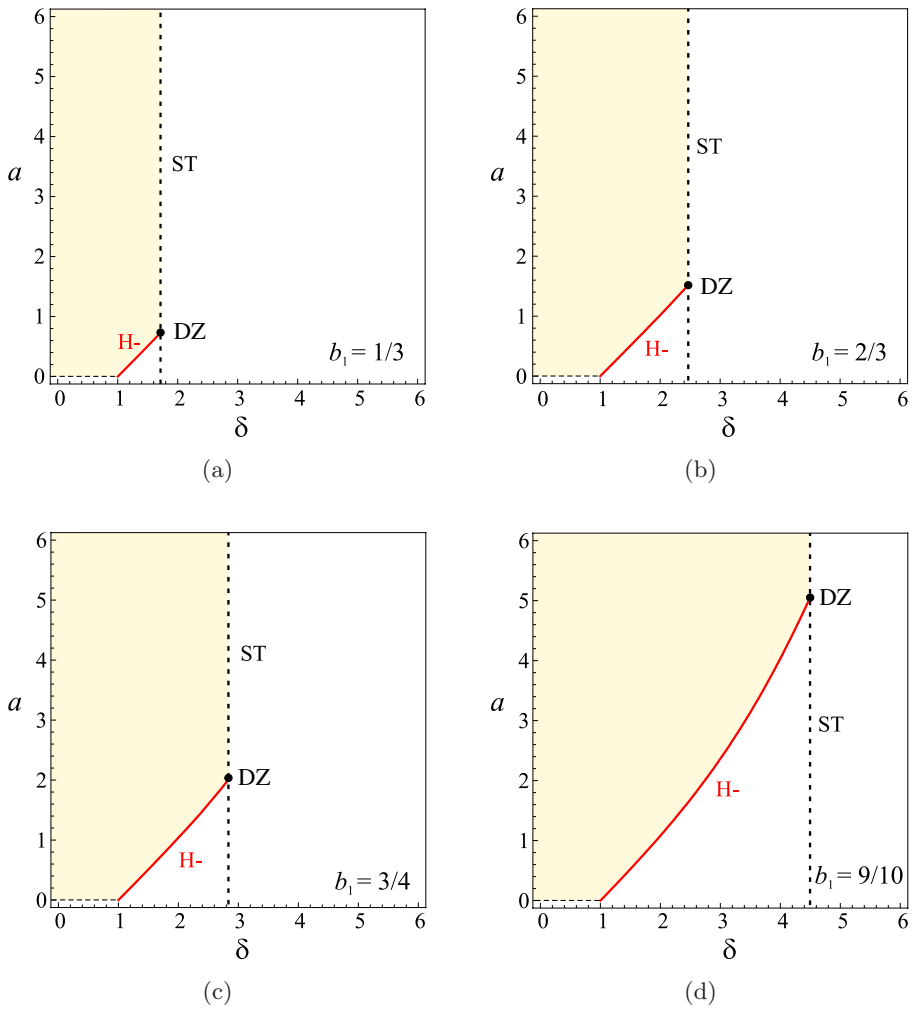

Fig. 3. Bifurcation diagrams for system (29) with weak gamma kernel for $b_2 = 1/2$ and different values of b_1. In each case, the shaded region represents the stability region of the equilibrium point at zero.

the gamma kernel, it is simple to show that the mean delay defined in (3) results in $\tau_m = p/a$. Then, if b_1 and b_2 are fixed, $\tau_m^{(\mathrm{DZ})}$ is given by (39) and the value of parameter a for which the DZ bifurcation occurs is $a^{(\mathrm{DZ})} = p/\tau_m^{(\mathrm{DZ})}$. For example, if $b_1 = 2/3$, $b_2 = 1/2$ and $p = 1$ then from (39), $\tau_m^{(\mathrm{DZ})} = 2/3$ and $a^{(\mathrm{DZ})} = 3/2$, as is shown in Fig. 3(b).

Notice that as a decreases (the mean delay increases) the stability region shrinks (i.e. the range of values of δ for which the origin is stable becomes narrower). Thus, as can be expected, an increase on the delay has a destabilizing effect on the system. Increasing either a_1 or a_2 also destabilizes the equilibrium point.

Remark. Notice that if $b_1 = 1$ or $b_2 = 1$ then $(\hat{x}_1, \hat{x}_2) = (0, 0)$ is the unique equilibrium point of (29). In this case, the condition for a static bifurcation (37) is never satisfied and obviously the DZ point does not exist. Then, the trivial equilibrium point can lose its stability through a Hopf bifurcation only. As a consequence, the stability region increases conforming b_1 or b_2 tends to unity.

In order to determine the direction and stability of the emerging periodic solutions, we refer to the Graphical Hopf Bifurcation Theorem (GHBT) [Mees & Chua, 1979; Moiola & Chen, 1996]. We compute the auxiliary complex number $\xi(\omega; \mu)$ appearing in (27). The calculations are a bit extensive and are given in the Appendix. Figure 4 shows two geometrical loci of $\hat{\lambda}(i\omega; \mu)$ and the corresponding ξ vectors for a stable (up) and unstable (down) trivial equilibrium. When the equilibrium point is unstable, the intersection between $\hat{\lambda}$ and ξ predicts the existence of a stable limit cycle according to

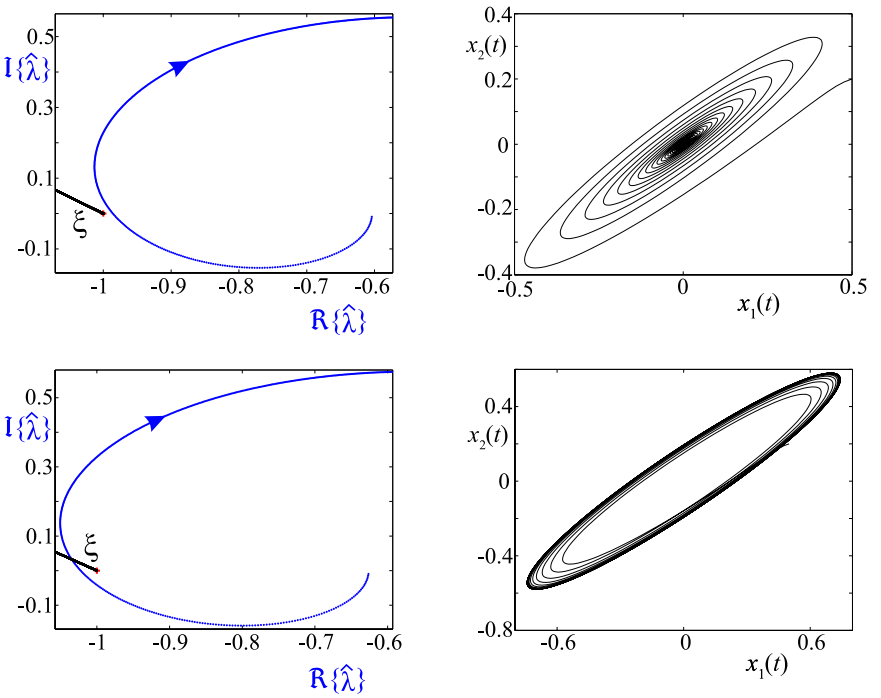

Fig. 4. Nyquist diagrams and numerical simulations for system (29) with weak gamma kernel, with $a = 2$, $b_1 = 9/10$, $b_2 = 1/2$ and $a_1 = a_2 = 2.7$ (up, stable equilibrium), $a_1 = a_2 = 2.8$ (down, unstable equilibrium).

the GHBT, which is also confirmed via numerical simulation. In this example, we choose $f(u) = \tanh(u)$ in (29).

In the following subsection, we will analyze the particular case in which $b_1 = b_2$, which we will call *symmetrical* case. In this situation, the bifurcation equations become more tractable and we can obtain analytical results for several gamma kernels.

3.3. *Symmetrical case* ($b_1 = b_2$)

In this case, we suppose that the weights of the past influence are identical for the two neurons ($b_1 = b_2 = b$). From (34), we obtain the solution in the variable λ as

$$\hat{\lambda}(s;\mu) = \delta\frac{[bK(s) - 1]}{s + 1}.$$

The static bifurcation condition (38) reduces to $\delta_{ST} = 1/|b - 1|$ and the DZ condition becomes $\tau_m^{(\mathrm{DZ})} = (1 - b)/b$, $0 < b < 1$. The Hopf bifurcation condition $\hat{\lambda}(i\omega_0;\mu) = -1$ leads to

$$a^p b\delta = (\delta - 1 - i\omega_0)(a + i\omega_0)^p. \qquad (47)$$

Table 1 summarizes the Hopf bifurcation conditions obtained by solving (47) for several values of p. In each case, that condition represents a curve formed by Hopf points in the (δ, a) plane. The corresponding bifurcation diagrams are depicted in Figs. 5(a)–5(c), where we picked $b = 1/2$.

Table 1. Hopf bifurcation condition in the parameter space, for the symmetrical case and different values of p.

p	Bifurcation Condition
1	$a = \delta - 1$
2	$ab\delta = 2(\delta - a - 1)^2$
3	$\omega_0^4 + 3a(\delta - a - 1)\omega_0^2 + a^3[\delta(b - 1) - 1] = 0$, where $\omega_0^2 = a^2[3(\delta - 1) - a]/[\delta - 1 - 3a]$.

Additionally, Eq. (27) allows to compute the approximate amplitude of a periodic solution arising from a Hopf bifurcation, for parameter values beyond the critical one. The algorithm used for this purpose is explained in the Appendix. Figure 6 compares the amplitude of the periodic solution approximated with the GHBT and the one obtained by numerical simulations carried out with Matlab. The amplitude is presented as function of δ for the case of the weak kernel, with $a = 1/2$ and $b_1 = b_2 = 1/2$. Notice that the amplitude of the limit cycle grows fast as the parameter δ increases beyond the critical value. Thus, we obtained approximations

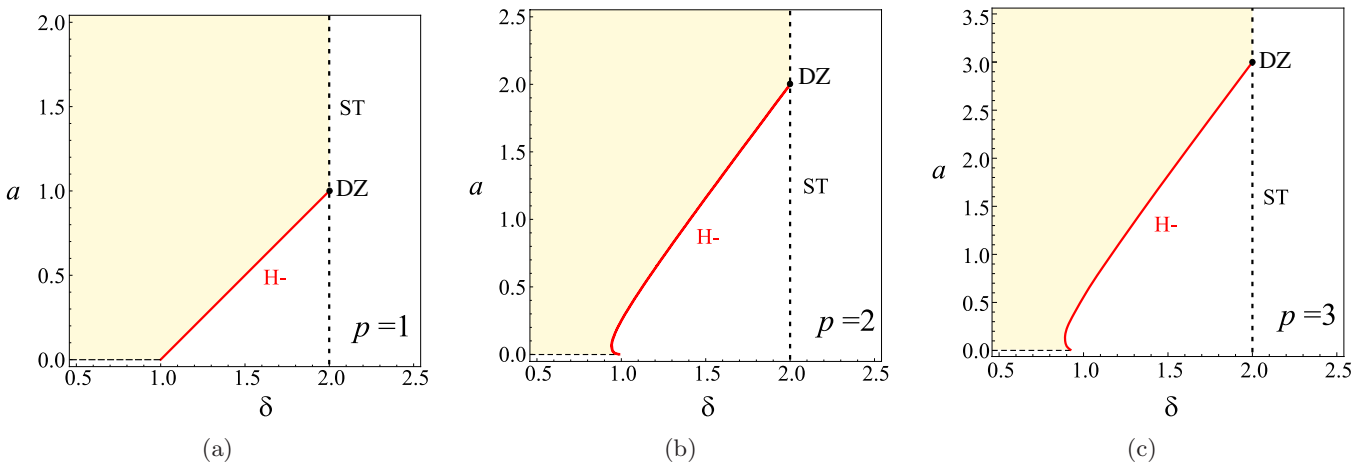

Fig. 5. Bifurcation diagrams for system (29) using gamma kernels with different values of p, with $b_1 = b_2 = 1/2$. Notice the different "a" axis scale in each case.

of oscillations whose amplitudes are not necessarily small.

3.4. *Dynamics near the double zero bifurcation*

In the previous subsections, we have shown several bifurcation diagrams representing the dynamics exhibited by the trivial equilibrium point. However, in each case, the DZ point not only unfolds curves of static and Hopf bifurcations, in fact, the dynamical scenario around it is by far more complicated. In order to be more specific, let us consider the activation function $f(u) = \tanh(u)$ in (29), as usual in the literature of neural networks. In this case, provided by the odd-symmetry of this function, system (29) becomes invariant under the change of variables given by $(x_1, x_2) \mapsto (-x_1, -x_2)$, i.e. it exhibits the so-called $\mathbb{Z}_2$ symmetry [Kuznetsov, 2004]. As a consequence, the ST curves shown in Figs. 3 and 5 represent Pitchfork bifurcations. Let us rewrite (32) as follows

$$\begin{cases} \hat{x}_1 = a_1 \tanh[(1 - b_2)\hat{x}_2], \\ \hat{x}_2 = a_2 \tanh[(1 - b_1)\hat{x}_1]. \end{cases} \tag{48}$$

It is simple to see that one or three equilibria can exist, depending on the values of the parameters a_1, a_2, b_1 and b_2. If there is a nonzero solution $\mathbf{x}_+ = (\hat{x}_1^{(1)}, \hat{x}_2^{(1)})$ of (48) with $\hat{x}_1^{(1)}, \hat{x}_2^{(1)} > 0$ then $\mathbf{x}_- = (-\hat{x}_1^{(1)}, -\hat{x}_2^{(1)})$ is also a solution. When the equilibrium points $\mathbf{x}_+, \mathbf{x}_-$ exist, their stability properties can be studied taking the state-space representation in (30) and the Jacobian matrix

$$J_{\pm}^*(\mu) = \begin{pmatrix} 0 & -a_1 f_2' & 0 & a_1 b_2 f_2' \\ -a_2 f_1' & 0 & a_2 b_1 f_1' & 0 \end{pmatrix},$$

where

$$f_1' \triangleq f'[(1 - b_1)\hat{x}_1^{(1)}] \quad \text{and}$$

$$f_2' \triangleq f'[(1 - b_2)\hat{x}_2^{(1)}].$$

The characteristic equation in the frequency domain for $\mathbf{x}_+$ and $\mathbf{x}_-$ becomes

$$\begin{aligned} h(\lambda, s; \mu) &= |\lambda I_4 - G^*(s) J_{\pm}^*(\mu)| \\ &= \frac{\lambda^2}{(s+1)^2}\{\lambda^2(s+1)^2 \\ &\quad - a_1 a_2 f_1' f_2' \eta_1(s)\eta_2(s)\} = 0 \end{aligned} \tag{49}$$

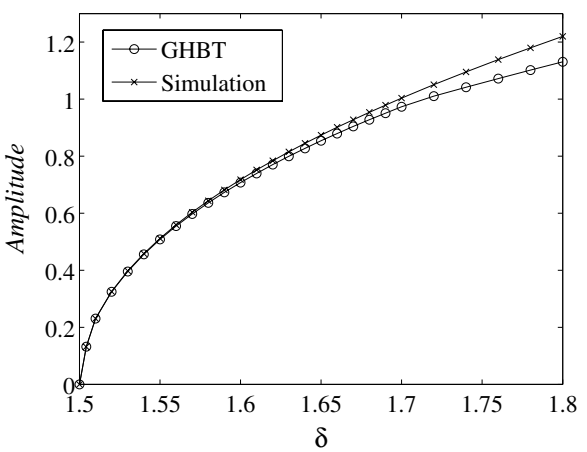

Fig. 6. Amplitude of the limit cycle arising from a Hopf bifurcation, with $p = 1$, $a = 1/2$, with $b_1 = b_2 = 1/2$. The curve labeled with crosses corresponds to numerical simulations and the one labeled with circles denotes the approximate amplitude obtained with the GHBT.

and the solution in the variable λ is obtained in similar form as that in (40) as

$$\hat{\lambda}(s;\mu) = \frac{\delta_1\sqrt{\eta_1(s)}\sqrt{\eta_2(s)}}{s+1}, \tag{50}$$

where $\delta_1 \triangleq \sqrt{a_1 a_2 f_1' f_2'}$. For example, let us consider $b_1 = 2/3$, $b_2 = 1/2$ and a weak gamma kernel, as in Fig. 3(b). Figure 7 shows an enlarged view near the double zero point, in which ST [obtained from (38)] and H$_-$ [computed using (46)] have the same meaning as that in Fig. 3. The curve H$_+$ represents Hopf bifurcations of the nontrivial equilibria, and it is obtained from (49) in similar fashion as H$_-$. The gray shaded area represents *qualitatively* the occurrence of two global phenomena which cannot be computed through the GHBT, but their existence is very well known. Actually, the expected dynamics around the double zero point for a $\mathbb{Z}_2$ symmetric system is described in detail in [Kuznetsov, 2004] and is shown in Fig. 9.10 of the cited book. In conclusion, we computed *analytically* the curves representing local bifurcation through the GHBT and showed *qualitatively* the global phenomena.

Let us consider Fig. 7 and suppose a counterclockwise movement around the double zero point. Starting from region I, the unique equilibrium at the origin is asymptotically stable. In region II, that equilibrium has lost its stability via a supercritical Hopf bifurcation, which has generated a stable limit cycle. In region III, a pitchfork bifurcation has led to two new equilibria, which are symmetrical from the origin and unstable. When crossing H$_+$ to region IV, a subcritical Hopf bifurcation turns the nontrivial equilibrium points stable, and both $\mathbf{x}_+$ and $\mathbf{x}_-$ are surrounded by "small" unstable limit cycles. When these limit cycles grow large enough, they collide with the origin forming a homoclinic "figure eight" orbit, which later separates from the origin and becomes a "big" unstable limit cycle having the three equilibria inside it. These two global phenomena occur inside region V which is indicated only qualitatively because these global phenomena cannot be computed through the GHBT or be detected by numerical simulations. Finally, the unstable limit cycle collides with the stable one which surrounds the whole scenario, and via a saddle-node of limit cycles they disappear. Then, in

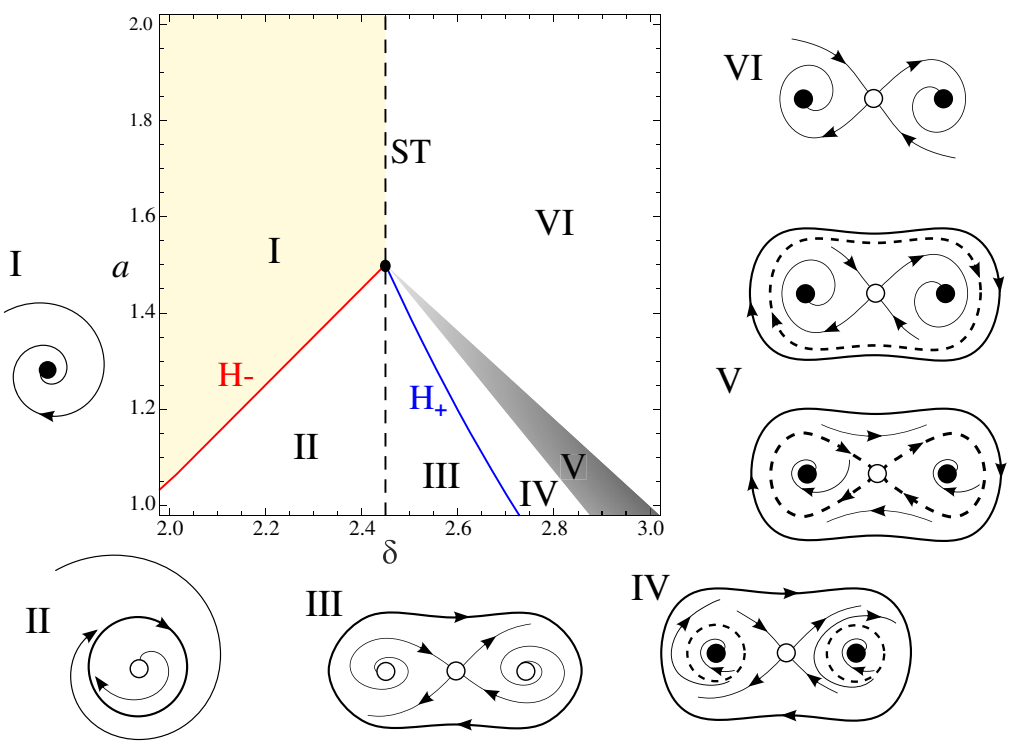

Fig. 7. Detail of the dynamics of system (29) near the double zero point. H$_-$ denotes the Hopf bifurcation of the equilibrium at zero and H$_+$ denotes Hopf bifurcations of the nontrivial equilibria. The gray shaded area (V) represents *qualitatively* the transition between the scenarios IV and VI. In the qualitative phase portraits, black points represent stable equilibria and white points unstable ones. The stable limit cycles are shown in black solid line and the unstable ones in dashed line.

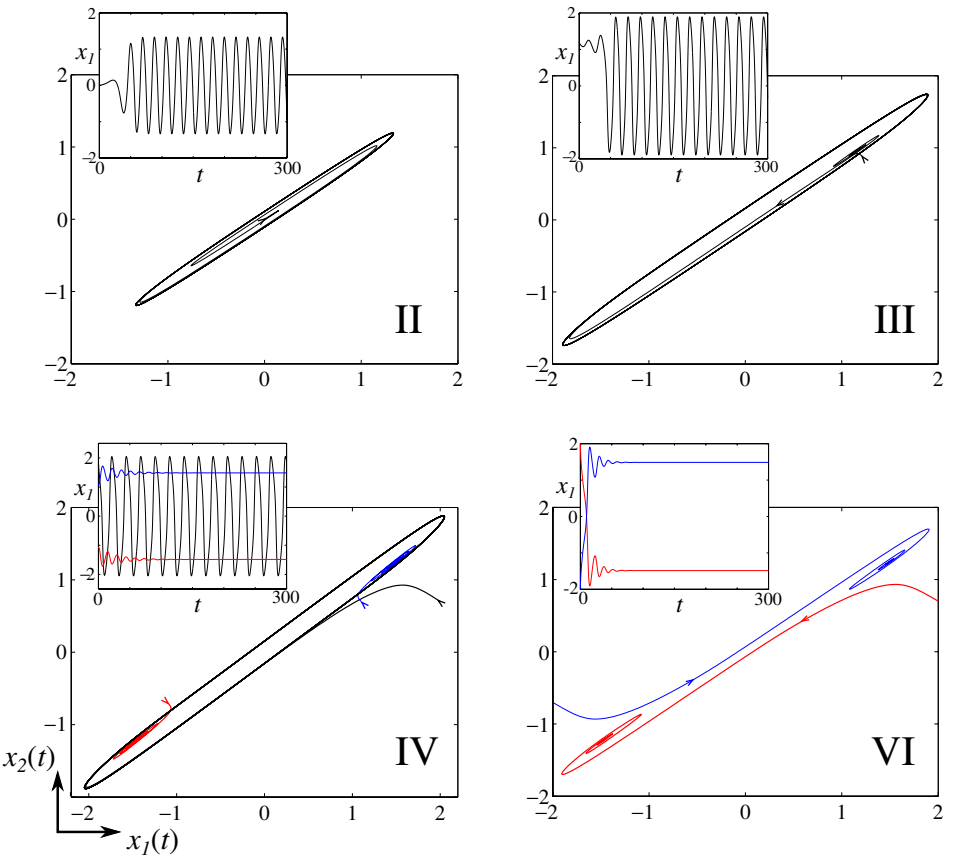

Fig. 8. Some numerical simulations corresponding to representative behaviors of regions in Fig. 7. For each region, we plotted a phase portrait and the time evolution of the variable x_1. Region II: $a = 1.2$, $\delta = 2.4$; initial values: $x_1(u) = 0$, $x_2(u) = 0.01$, $-\infty < u \leq 0$. Region III: $a = 1.1$, $\delta = 2.6$; initial values: $x_1(u) = 1.2$, $x_2(u) = 0.9$, $-\infty < u \leq 0$. Region IV: $a = 1.1$, $\delta = 2.7$; initial values: $x_1(u) = 1.1$, $x_2(u) = 0.7$, $-\infty < u \leq 0$ for the trajectory tending to $\mathbf{x}_+$ (blue); $x_1(u) = -1.1$, $x_2(u) = -0.7$, $-\infty < u \leq 0$ for the trajectory tending to $\mathbf{x}_-$ (red) and $x_1(u) = 2$, $x_2(u) = 0.7$, $-\infty < u \leq 0$ for the trajectory tending to the "big" limit cycle. Region VI: $a = 1.2$, $\delta = 2.7$; initial values: $x_1(u) = 2$, $x_2(u) = 0.7$, $-\infty < u \leq 0$ for the trajectory tending to $\mathbf{x}_-$ (red) and $x_1(u) = -2$, $x_2(u) = -0.7$, $-\infty < u \leq 0$ for the trajectory tending to $\mathbf{x}_+$ (blue). The small arrows indicate the direction of the flow.

region VI, only the three equilibria remain. When crossing the ST curve again, the stable equilibria $\mathbf{x}_+$ and $\mathbf{x}_-$ collide at the origin through a pitchfork bifurcation, and we return to the situation of region I.

It is worth mentioning that a similar dynamical behavior has been found in [Fan *et al.*, 2013] also in a system of two coupled neurons, but each with a delayed self feedback and a delayed connection from the other neuron. The authors considered concentrated (point) delays instead of distributed ones.

Figure 8 shows numerical simulations illustrating the behaviors corresponding to regions II, III, IV and VI of Fig. 7. For each region, we plotted a phase portrait together with the time evolution of the variable x_1. In regions II and III, we considered different initial functions in order to show trajectories converging to each of the existing attractors.

4. Conclusions

In this work, we presented a modified version of the GHBT which allows the bifurcation analysis of DDEs with distributed delays. This approach takes advantage of a simple interpretation of the effect of the distributed delay based on the Laplace transform properties. Thus the main advantage of our approach is the reutilization of a very well known technique (originally meant to study ODEs) to analyze systems with distributed delays, without the need for formulating an equivalent system, which is not always possible. The proposed methodology does not depend on the particular shape of

the distribution function (notice that in the example, we derived the characteristic equation without choosing a particular kernel) and at this point our approach distinguishes from the existing works (see, for example [Liao *et al.*, 2004; Xiao *et al.*, 2013]). Finally, it is worth to mention that the proposed approach can be easily extended to the case of multiple delays.

The theoretical results were illustrated through an example consisting of two coupled neurons, for which we have obtained bifurcation diagrams of the trivial equilibrium point for several gamma kernels in the symmetrical (simpler) case and the weak gamma kernel in the asymmetric (general) case. In addition, we stated analytical conditions for the appearance of a double zero bifurcation, which in turn unfolds a pitchfork bifurcation of equilibria and Hopf bifurcations of both the trivial and nontrivial equilibria. For completeness, we analyzed the behavior of the system near the double zero point, and we found a similar scenario as the one described in Fig. 9.10 of [Kuznetsov, 2004] and in [Fan *et al.*, 2013].

Acknowledgment

The authors is grateful for the financial support of the following grants: PICT 2010-0465 (ANPCyP), PIP 112-201201-00144 (CONICET) and PGI 24/K064 (UNS).

References

Arino, J. & van der Driessche, P. [2006] "Time delays in epidemic models: Modelling and numerical considerations," *Delay Differential Equations and Applications*, eds. Arino, J. *et al.* (Springer), pp. 539–578.

Atay, F. M. [2003] "Distributed delays facilitate amplitude death of coupled oscillators," *Phys. Rev. Lett.* **91**, 094101(1–4).

Bernard, S., Bélair, J. & Mackey, M. C. [2001] "Sufficient conditions for stability of linear differential equations with distributed delay," *Discr. Contin. Dyn. Syst. Ser. B* **1**, 233–256.

Cao, J. & Xiao, M. [2007] "Stability and Hopf bifurcation in a simplified BAM neural network with two time delays," *IEEE Trans. Neural Netw.* **18**, 416–430.

Crauste, F. [2010] "Stability and Hopf bifurcation for a first-order delay differential equation with distributed delay," *Complex Time-Delay Systems*, ed. Atay, F. M. (Springer), pp. 263–296.

Culshaw, R. V., Ruan, S. & Webb, G. [2003] "A mathematical model of cell-to-cell spread of HIV-1 that includes a time delay," *J. Math. Biol.* **46**, 425–444.

Fan, G., Campbell, S. A., Wolkowicz, G. S. K. & Zhu, H. [2013] "The bifurcation study of 1:2 resonance in a delayed system of two coupled neurons," *J. Dyn. Diff. Eqs.* **25**, 193–216.

Gentile, F. S., Moiola, J. L. & Paolini, E. E. [2012] "On the study of bifurcations in delay-differential equations: A frequency-domain approach," *Int. J. Bifurcation and Chaos* **22**, 1250137-1–15.

Gopalsamy, K. & He, X. Z. [1994] "Delay-independent stability in bidirectional associative memory networks," *IEEE Trans. Neural Netw.* **5**, 998–1002.

Hajihosseini, A., Lamooki, G. R. R., Beheshti, B. & Maleki, F. [2010] "The Hopf bifurcation analysis on a time-delayed recurrent neural network in the frequency domain," *Neurocomputing* **73**, 991–1005.

Kuznetsov, Y. A. [2004] *Elements of Applied Bifurcation Theory*, 3rd edition (Springer-Verlag, NY).

Liao, X., Wong, K. W. & Wu, Z. [2001] "Bifurcation analysis on a two-neuron system with distributed delays," *Physica D* **149**, 123–141.

Liao, X., Li, S. & Wong, K. [2003] "Hopf bifurcation on a two-neuron system with distributed delays: A frequency-domain approach," *Nonlin. Dyn.* **31**, 299–326.

Liao, X., Li, S. & Chen, G. R. [2004] "Bifurcation analysis on a two-neuron system with distributed delays in the frequency-domain," *Neural Netw.* **17**, 545–561.

Liu, Y., Wang, Z. & Liu, X. [2006] "Global exponential stability of generalized recurrent neural networks with discrete and distributed delays," *Neural Netw.* **19**, 667–675.

Mees, A. I. & Chua, L. O. [1979] "The Hopf bifurcation theorem and its applications to nonlinear oscillations in circuits and systems," *IEEE Trans. Circuits Syst.* **26**, 235–254.

Moiola, J. L. & Chen, G. R. [1996] *Hopf Bifurcation Analysis*: *A Frequency Domain Approach* (World Scientific, Singapore).

Rasmussen, H., Wake, G. C. & Donaldson, J. [2003] "Analysis of a class of distributed delay logistic differential equations," *Math. Comput. Model.* **38**, 123–132.

Ruan, S. & Filfil, R. S. [2004] "Dynamics of a two-neuron system with discrete and distributed delays," *Physica D* **191**, 323–342.

Ruan, S. [2006] "Delay differential equations in single species dynamics," *Delay Differential Equations and Applications*, eds. Arino, J. *et al.* (Springer), pp. 477–517.

Tank, D. W. & Hopfield, J. J. [1987] "Neural computation by concentrating information in time," *Proc. Natl. Acad. Sci. USA* **84**, 1896–1900.

Unnikrishnan, K. P., Hopfield, J. J. & Tank, D. W. [1991] "Connected-digit speaker-dependent speech recognition using a neural network," *IEEE Trans. Sign. Process.* **39**, 698–713.

Xiao, M., Zheng, W. X. & Cao, J. [2013] "Frequency domain approach to computational analysis of bifurcation and periodic solution in a two-neuron network model with distributed delays and self-feedbacks," *Neurocomputing* **99**, 206–213.

Yu, W., Cao, J. & Chen, G. R. [2008] "Stability and Hopf bifurcation of a general delayed recurrent neural network," *IEEE Trans. Neural Netw.* **19**, 845–854.

Yuan, Y. & Bélair, J. [2011] "Stability and Hopf bifurcation analysis for functional differential equation with distributed delay," *SIAM J. Appl. Dyn. Syst.* **10**, 551–581.

Zhang, J. & Jin, X. [2000] "Global stability analysis in delayed Hopfield neural network models," *Neural Netw.* **13**, 745–753.

Appendix A

Procedure for Computing ξ

Here we provide some details on the procedure for obtaining the complex number ξ appearing in (27), which is needed to know the direction and stability of the limit cycle generated by the Hopf bifurcation, according to the GHBT given in [Mees & Chua, 1979]. The first step consists of computing the right and left eigenvectors of matrix $G^*(s)J^*(\mu)$. Considering matrices $G^*(s)$ from (31) and $J^*(\mu)$ from (33), we obtain those eigenvectors as

$$\mathbf{v} = (v_1(s), 1, v_1(s)K(s), K(s))^T$$
$$\mathbf{u} = (u_1(s), -1, -u_1(s)b_1, b_2)^T,$$

where

$$v_1(s) \triangleq \frac{a_1 f'}{\delta}\sqrt{\frac{\eta_2(s)}{\eta_1(s)}}, \quad u_1(s) \triangleq -\frac{a_2}{a_1}v_1(s). \quad \text{(A.1)}$$

The second step consists of computing $H^*(s;\mu)$ from (24) and

$$\mathbf{v}_0 = -\frac{1}{4}H(0;\mu)(\mathfrak{D}^2\mathbf{g})\mathbf{v}\otimes\overline{\mathbf{v}},$$
$$\mathbf{v}_2 = -\frac{1}{4}H(i2\omega;\mu)(\mathfrak{D}^2\mathbf{g})\mathbf{v}\otimes\mathbf{v}, \quad \text{(A.2)}$$

which are equivalent to the quantities in (23) but scaled by $1/\theta^2$. We compute (A.2) instead of (23) because the quantity θ is unknown yet, and it can be obtained at the end of the procedure. The true amplitudes of the Fourier coefficients are recovered easily from the following relationships

$$\mathcal{Y}^{0*} = \theta^2\mathbf{v}_0, \quad \mathcal{Y}^{1*} = \theta\mathbf{v}, \quad \mathcal{Y}^{2*} = \theta^2\mathbf{v}_2.$$

Then, vector $\mathbf{p}(\omega;\mathbf{v})$ in (27) is given by

$$\mathbf{p}(\omega,\mathbf{v}) \triangleq (\mathbf{D}^2\mathbf{g})[\mathbf{v}_0\otimes\mathbf{v} + \overline{\mathbf{v}}\otimes\mathbf{v}_2] + \frac{1}{8}(\mathbf{D}^3\mathbf{g})\mathbf{v}\otimes\mathbf{v}\otimes\overline{\mathbf{v}}. \quad \text{(A.3)}$$

For the case presented in Sec. 4.2, the matrix of second-order derivatives given by (13)–(19) is null, then the zero and second harmonic components (A.2) are zero. Then, $\mathbf{p}(\omega;\mathbf{v})$ in (A.3) results in

$$\mathbf{p}(\omega;\mathbf{v}) = \frac{1}{4}\begin{pmatrix} a_1\eta_2(i\omega)|\eta_2(i\omega)|^2 \\ a_2\eta_1(i\omega)|\eta_1(i\omega)|^2|v_1(i\omega)|^2 \end{pmatrix} \quad \text{(A.4)}$$

and from (28), the auxiliary vector ξ is given by

$$\xi(\omega;\mu) = \frac{\eta_1\eta_2(a_2v_1|v_1|^2|\eta_1|^2 + a_1u_1|\eta_2|^2)}{4(1+i\omega)(\eta_1+\eta_2)},$$

where we have omitted the argument $i\omega$ in η_1, η_2, v_1 and u_1 for short. After replacing (A.1) into (A.4) and making several simplifications we finally arrive at

$$\xi(\omega;\mu) = \frac{a_1|\eta_1|\sqrt{\eta_1\eta_2}(a_1|\eta_1| - a_2|\eta_2|)}{8|K(i\omega)|^2\sqrt{a_1a_2}(1+i\omega)}. \quad \text{(A.5)}$$

In order to obtain an approximation of the amplitude of the limit cycles, we must find the pair (ω,θ) that solves (27). This task can be performed by an iterative process, starting from ω_0, the frequency at which $\hat{\lambda}(i\omega;\mu_0)$ crosses the $-1+i0$ point. If μ is close enough to μ_0, the true frequency ω remains close to ω_0 [Mees & Chua, 1979]. Then, we first compute $\xi(\omega_0;\mu)$ and use the following algorithm

$$\begin{aligned}
&\text{(Step 1)} && \hat{\lambda}(i\omega_1;\mu) = -1 + \xi(\omega_0;\mu)\theta_1^2,\\
&\text{(Step 2)} && \hat{\lambda}(i\omega_2;\mu) = -1 + \xi(\omega_1;\mu)\theta_2^2,\\
&\quad\vdots && \quad\vdots\\
&\text{(Step } N\text{)} && \hat{\lambda}(i\omega_N;\mu) = -1 + \xi(\omega_{N-1};\mu)\theta_N^2,
\end{aligned}$$

taking N large enough so that $|\omega_N - \omega_{N-1}| < \epsilon$, with ϵ very small. Finally, we assign $\omega := \omega_N$ and $\theta := \theta_N$. This procedure is performed for every fixed value of μ for which we want to approximate the amplitude of the limit cycle. In this way, we have obtained the results shown in Fig. 6.